www.rericjournal.ait.ac.th

Global and Diffuse Solar Radiation Characteristics of Bangkok and its Forecast Using Artificial Neural Network

Natthanan Chawphongphang*, Pipat Chaiwiwatworakul*, #, 1, and Surapong Chirarattananon*, #

ARTICLE INFO

Article history:
Received 03 May 2022
Received in revised form
29 August 2022
Accepted 13 September 2022

Keywords:
Artificial neural network
Diffuse radiation
Forecast
Global radiation
Tropical

ABSTRACT

This paper investigated the artificial neural network (ANN) modeling to forecast the one-hour ahead global and diffuse solar radiation using the observed data during 2019-2021 at a meteorological station in Bangkok, Thailand. Results from the statistical analysis portrayed the abundance of the tropical solar radiation and its large variation all year round. As a step to move advance the renewable energy use of the solar radiation at the location, the ANN forecasting models were proposed for all climatic conditions. The model input were the ambient temperature, solar elevation, and an insolation parameter namely normalized global solar radiation. The model performance was assessed by using the two statistic parameters: normalized mean bias error (nMBE), and normalized root mean square error (nRMSE). The results showed that the ANN models could forecast the global radiation with the nMBE of 1.79% and nRMSE of 26.20%. For the diffuse radiation forecast, the nMBE and nRMSE of the models were obtained at 7.78% and 36.21%, respectively. In order to demonstrate a benefit of the two developed ANN models, their forecasted horizontal data were employed to further predict the total solar radiation on vertical plane. Benchmarked with the smart persistence model, the developed ANN models possessed the higher forecasting accuracy for all weather conditions.

1. INTRODUCTION

Globally, the building sector consumed 35% of the end-use energy and contributed 39% of the emitted greenhouse gas (GHG) [1]. The net-zero and the ultra-low energy buildings are introduced as a promising solution to curb the raise of the sectoral energy consumption. On the one hand, the passive building design and the active energy efficient devices are implemented to the buildings to minimize the building energy demand. On the other hand, the photo-voltaic (PV) systems are installed on the building roofs and the facades for the on-site power generation. Due to the rapid decrease of the PV panel price, the PV installations are now growing, and result in increasing the solar power leading to the decarbonization in the electricity sector. Even though it was perceived that the solar power is environmentally friendly, its intermittent behavior could cause the adverse effect on the difficulty and complexity to the existing power plant operation and the grid management. The solar radiation also greatly influences the external heat gain of the building air-conditioning, the indoor thermal comfort, and sequentially the optimal chiller's plant control. Regarding the above issues, solar forecasting is a potential technology that helps managing the building systems, maximizing the solar power utilization, and stabilizing the instantaneous power in the grid system [2].

Routine measurement of the global solar radiation has been widely carried out in middle latitude countries [3]. In Southeast Asia, the measurements were found in Malaysia [4], Singapore [5], and Indonesia [6]. In Thailand, the global radiation has been measured for decades, and the records were used to develop Thailand's solar radiation map [7]. Other than establishing the radiation databases, forecasting of the solar radiation using computational models for a future time horizon is essential to enhance balancing between the building energy demand and the solar power generation. Different forecasting methods were investigated and developed in prior research works and they could be categorized into four methods that are physical model, empirical model, statistical model, and machine learning model [8].

The physical models, so called the numeric weather prediction (NWP) models, employ dynamics and physics equations of the atmosphere to forecast future weather *e.g.*, solar radiation, ambient temperature, and wind velocity. Mathiesen and Kleissl [9] developed a NWP model using the solar zenith and sky ratio as the model input to forecast the intraday solar radiation in the continental United States. The model offered a forecasting performance with a root mean square error (RMSE) of 85 W/m^2. Gamarro *et al.* [10] proposed an urban-specific

*The Joint Graduate School of Energy and Environment, King Mongkut's University of Technology Thonburi, Bangkok, Thailand.

#Center of Excellence on Energy Technology and Environment (CEE), Ministry of Higher Education, Science, Research and Innovation (MHESI), Bangkok, Thailand.

[1]Corresponding author;
Tel: + 66 816592535
E-mail: pipat.cha@kmutt.ac.th; pipatc@gmail.com

NWP model for the global radiation forecast in New York, USA. The proposed model had the coefficient of determination (R^2) of 0.93, 0.61 and 0.39 for clear sky, partly cloudy sky, and overcast sky, respectively. A NWP model was introduced by Böök and Lindfors to forecast photovoltaic power production [11]. The model was accompanied with the site-specific adjustment to enhance the model's accuracy. A major drawback of the physical method is the requirement of large computing resources [12]. Imperfect weather data in most locations limited the application of this method.

Empirical model is a simple method of the solar forecast; however, accuracy of the empirical model is usually limited [13]. Ibrahim *et al.* [14] developed a regressed model to estimate the solar radiation using ambient air temperature in Malaysia. The model performance was relatively low with the R^2 value of 0.5585. The method also seemed suitable for data fitting rather than data forecasting.

The statistical regression presents an alternative method of the solar forecast. Mbaye et al. [15] used the autoregressive moving average (ARMA) model to forecast the short term global radiation for Dakar-Fann, Senegal. This model was developed using the one-year data and could provide the prediction accuracy with RMSE of 0.629 W/m^2 and R^2 of 0.963. The mean absolute error (MAE) and the mean bias error (MBE) were obtained at 0.528 W/m^2 and 0.012 W/m^2, respectively. However, the limitation of statistical techniques is that they mostly used linear transformation, but the solar radiation relationship was nonlinear.

Literature reported that the solar forecasting using machine learning outperformed other traditional methods [16]. Ağbulut *et al.* [17] assessed the forecasting performance of four Artificial Intelligence (AI) techniques: Artificial Neuron Network (ANN), Support Vector Machine (SVM), k-Nearest Neighbors (k-NN), and Deep Learning (DL) for the daily global radiation for four locations in Turkey. The model input was the daily minimum and maximum of the ambient temperature, cloud cover, extraterrestrial solar radiation, daylength, and solar radiation. The results exhibited that the ANN model outperformed other techniques. The DL method came the second, followed by the SVM and k-NN. For another study in Australia, Ghimire *et al.* [18] evaluated the ANN model performance against other models of support vector regression (SVR), Gaussian process machine learning (GPML), and genetic programming (GP) to forecast the daily global radiation. This work demonstrated the consistent results that the ANN model was superior to the others (SVR, GPML, and GP) and recommended the ANN model to be tested its performance in sub-tropical region.

In France, Notton *et al.* [19] proposed the ANN prediction models of the hourly beam and the hourly global radiation for the time horizon of one-hour ahead up to six hours ahead at Bouzareah. The model input included the ten parameters of temperature and relative humidity of the ambient air, wind velocity and direction, water precipitation, sunshine duration, atmospheric pressure, declination, solar angle, and extraterrestrial solar radiation. The analysis showed that the performance of proposed ANN models that gave in terms of the normalized root mean square error (nRMSE) were 22.57% for one-hour ahead prediction and 34.85% for six-hour ahead prediction. Another study of Notton *et al.* [20] applied the ANN models to forecast the total radiation on tilted surfaces at angle of 45° and 60° from the ground using the data input of the declination, time, solar zenith angle, extraterrestrial horizontal radiation, and global horizontal radiation. Again, the ANN model performed slightly better than the traditional method of empirical correlations.

Premalatha and Valan Arasu [21] conducted a study of the ANN models to forecast the monthly average global radiation for five provinces in India using the 10-year meteorological records. The model inputs included the geometrical parameters of the latitude, longitude, and altitude of the locations, and the meteorological data of the mean values of the ambient air temperature, relative humidity, wind velocity, and station level pressure. The work investigated the effects of four back propagation algorithms, namely gradient descent (GD), Levenberg–Marquardt (LM), Scaled conjugate gradient (SCG), and Resilient back propagation (RP) on the model forecasting accuracy. The results indicated the LM algorithm offered the best accuracy compared to the others (GD, SCG, and RP). Further, the study confirmed the forecasting accuracy of the ANN models relied on the number and the variety of trained data.

Another study in India developed an ANN forecasting model for the diffuse solar radiation [22]. The data were acquired from 10 meteorological stations. The model input was the site's location (*i.e.*, latitude, longitude, and altitude), ambient temperature, relative humidity, rainfall amount, and wind velocity. The feedforward back-propagation algorithm was used in the model development. The model accuracy was assessed against existing parametric models using RMSE. The study revealed that the ANN model was more suitable for forecasting the monthly mean hourly value of diffuse solar radiation for Indian. The ANN model was more accurate and versatile than other well-published parametric models chosen for the evaluation.

In Thailand, monthly mean global radiation was studied and estimated by an ANN model [23]. The model used the monthly values (maximum, minimum, and mean) of the ambient temperature, relative humidity, rainfall amount, and sunshine duration as the input. The model gave an RMSE of 0.0031 to 0.3632 MJ/m^2/day and an MBE of -0.0203 to 0.003 MJ/m^2/day, indicating that the ANN model had the adequate accuracy of forecasting the monthly mean global radiation of Thailand.

Most of the ANN modeling focused on forecasting the global radiation some of which limited to a particular condition of the clear sky [24]. It was observed that fewer studies were carried out for the diffuse component of which the prediction was more difficult due to the random moving clouds [22], [25]. The individual ANN models possessed different required input which were dependent on the available site's data. The model outputs were also different with regard to the distinct forecasting time scale *e.g.*, monthly, daily, hourly, or a very short time step of 5-10 minutes. In real practices, many analyses of energy

systems such as energy conversion of the PV systems and of the thermal solar collectors, or the calculation of the external building cooling load would require the radiation data on tilted surfaces. In this case, the calculation would be more complicated due to which the surfaces were facing to only particular part of the sky and the actual luminance distribution over the sky vault was anisotropic. The transposition model is a traditional method to determine the total solar radiation on tilted surfaces. However, the procedure required the horizontal data of both the global and the diffuse solar radiation. By this context, adopting the existing ANN models to predict the tilted solar radiation was challenge due to the mismatch of the required model input and the output with the available data at the considered location.

This paper worked on the ANN modelling to forecast the global and the diffuse horizontal solar radiation, and the use of the two forecasted data to predict the total radiation on a vertical surface. The characterization of the global and diffuse solar radiation of Bangkok using observations from a meteorological station was carried out at the first step. The ANN solar forecasting models of both global and diffuse horizontal radiation were then developed based on the validated available databases. A comparison of the developed model performance was made against some prior models of other author's works. Lastly, a deployment of the developed ANN models together with a localized transposition model to predict the solar radiation on the south orientation was demonstrated. The study results showed that the prediction accuracy from the ANN model were more accurate that the smart persistent model.

2. SOLAR RADIATION CHARACTERISTICS

2.1 Measuring Station

The solar radiation data in this study were collected from a meteorological station erected on the roof deck of a seven-story building in the King Mongkut's University of Technology, Thonburi (KMUTT). The station site was at Bang Khun Tien campus in the southern outskirts area of Bangkok metropolis, Thailand (latitude 13.58°N and longitude 100.11°E). The global solar radiation (E_{eg}) was measured at the station using a CM-11 pyranometer supplied by Kipp&Zonen. The diffuse horizontal radiation (E_{ed}) was measured by another pyranometer placed on a sun tracker where a tracking ball automatically moved to shade the beam radiation from the sensor. A pyheliometer of the CHP1 model by Kipp&Zonen was equipped with the sun tracker to measure the beam normal radiation (E_{eb}). The radiation sensors were the secondary standard of the ISO 9060 and world meteorological organization (WMO) classification. According to the specification, the linearity of the sensors was 0.0% in the range of 0-500 W/m^2, and 0.7% at 1000 W/m^2. The cosine error was less than 3% at 10° sun altitude. The temperature dependence was +1% over the ambient temperature range of 10-40°C. The time respond was less than 5 second. The station also monitored the ambient condition including air temperature (T_a), relative humidity (RH_a), and wind speed (V_a). The temperature sensor had a measurement range of -32.9°C to 60°C with the accuracy of $\pm$0.2°C at 20°C. The relative humidity sensor had the output scale of 0-100% with the temperature dependence of $\pm$0.05%RH/°C.

All measurements were recorded every one-minute interval by a data logger. In this study, the three-year data were obtained from January 2019 to December 2021. Figure 1 illustrates a photo of the station. As observed, the station was located in open space; no obstruction nearby the station affecting the measurements.

Fig. 1. The meteorological station where the radiation data were compiled for this study.

2.2 Data Quality Control

The measured radiation data at the station were subject to a procedure of data quality assurance. The procedure comprised two tests carried out in series. For the first test, the measured radiation was checked and would be screened out if their values exceeded the extraterrestrial solar radiation. The remaining data were next evaluated by the second test of the data consistency check. As the station measured the global, diffuse horizontal and beam normal radiation, the consistency check could be performed by which the calculated values of the global radiation from the diffuse and beam components were to be compared to the corresponding global measurements.

The difference of the two values should be limited within ±10% of the measurement for the compliance with the second test. By this way, the spurious data from sensor malfunction and large calibration drift were expected to be eliminated by the second test. Only the data passing both tests were considered to be valid and could be used for the forecasting model development.

2.3 Solar Radiation Availability

Based on the validated data, statistical analysis was undertaken to characterize the solar radiation of Bangkok. Table 1 presents the numeric values of the hourly mean of the tropical global radiation for twelve calendar months. The hourly mean values of the diffuse horizontal radiation are given in Table 2. Their iso-contour plots are provided in Figures A.1 and A.2 in Appendix. At the header of Tables 1 and 2, M1 to M12 stand for January to December months.

The first observation from the data in the tables was the small difference of the daylength in the June solstice compared to the December solstice. As the study's site located in the tropics, the solar radiation amounts were high all year round. The seasonal variation could be noticed where the clear sky appeared most time in the dry period of November and December. The sky remained rather clear till April. The solar altitude angle reached 90 degrees twice a year; in April and in August. With this regard, the global radiation was maximum during April, while the diffuse amount was peak in August, the rainy season. According to the records, the monthly peak value of the global radiation was 859 W/m^2, and that of the diffuse horizontal was 419 W/m^2. The diffuse component shared about half of the global radiation. In [7], the radiation database from a station located inland 40km north of Bangkok was presented. By comparing with our results, the measured global radiation from both sites were quite consistent in terms of their variation patterns and magnitudes. However, it was not the case of diffuse horizontal radiation where our values were higher. The high diffuse radiation observed at our station was possibly the presence of bright clouds in most daytime as the station itself was situated close to gulf of Thailand. The radiation distinction between the two stations advised more solar stations to be installed. This also encouraged the necessity of mathematical model development for solar forecasting.

3. SOLAR RADIATION FORECAST

3.1 Artificial Neural Network Model

The next research task was to develop the forecasting model for the one-hour ahead solar radiation using the validated radiation database of southern Bangkok. This study adopted artificial neural network (ANN) as the forecasting technique due to its great prediction accuracy evidently reported by literature from different climates and localities.

Table 1. Monthly means hourly values of the measured global radiation (W/m^2).

Time	M1	M2	M3	M4	M5	M6	M7	M8	M9	M10	M11	M12
1	-	-	-	-	-	-	-	-	-	-	-	-
2	-	-	-	-	-	-	-	-	-	-	-	-
3	-	-	-	-	-	-	-	-	-	-	-	-
4	-	-	-	-	-	-	-	-	-	-	-	-
5	-	-	-	-	-	-	-	-	-	-	-	-
6	-	1	6	18	36	37	24	16	17	15	10	2
7	48	66	122	182	196	196	158	136	149	141	133	71
8	238	250	300	354	374	390	330	308	317	319	326	265
9	428	441	492	560	547	585	502	504	500	479	493	446
10	587	632	668	713	693	700	652	620	622	605	599	577
11	686	773	803	816	796	773	748	689	708	685	650	646
12	719	818	859	852	815	780	762	705	728	638	655	661
13	690	799	844	843	806	745	709	690	705	576	596	597
14	585	699	755	707	683	656	602	593	591	448	495	489
15	451	538	587	565	588	502	461	444	444	333	346	351
16	269	346	372	365	401	327	309	283	252	167	168	187
17	90	142	161	168	189	163	147	121	99	45	39	47
18	3	11	16	17	25	26	28	16	6	-	-	-
19	-	-	-	-	-	-	-	-	-	-	-	-
20	-	-	-	-	-	-	-	-	-	-	-	-
21	-	-	-	-	-	-	-	-	-	-	-	-
22	-	-	-	-	-	-	-	-	-	-	-	-
23	-	-	-	-	-	-	-	-	-	-	-	-
24	-	-	-	-	-	-	-	-	-	-	-	-

Table 2. Monthly means hourly values of the measured diffuse horizontal radiation (W/m^2).

Time	M1	M2	M3	M4	M5	M6	M7	M8	M9	M10	M11	M12
1	-	-	-	-	-	-	-	-	-	-	-	-
2	-	-	-	-	-	-	-	-	-	-	-	-
3	-	-	-	-	-	-	-	-	-	-	-	-
4	-	-	-	-	-	-	-	-	-	-	-	-
5	-	-	-	-	-	-	-	-	-	-	-	-
6	-	-	3	13	26	30	24	22	14	13	7	2
7	35	48	78	107	116	117	105	109	104	99	82	52
8	113	130	164	187	187	205	197	226	199	193	162	137
9	197	191	242	245	226	273	279	346	279	270	222	209
10	307	241	289	272	271	296	330	385	320	326	278	273
11	233	248	303	294	287	330	370	413	349	340	310	262
12	239	258	299	284	295	334	370	419	359	330	318	270
13	252	253	277	258	284	325	355	399	339	297	294	281
14	300	234	246	240	269	294	315	360	307	247	250	283
15	262	201	205	227	230	248	259	296	259	203	198	222
16	146	150	156	171	176	191	191	204	173	127	118	132
17	63	78	89	100	106	111	110	100	79	40	34	41
18	3	10	14	14	20	24	27	24	5	-	-	-
19	-	-	-	-	-	-	-	-	-	-	-	-
20	-	-	-	-	-	-	-	-	-	-	-	-
21	-	-	-	-	-	-	-	-	-	-	-	-
22	-	-	-	-	-	-	-	-	-	-	-	-
23	-	-	-	-	-	-	-	-	-	-	-	-
24	-	-	-	-	-	-	-	-	-	-	-	-

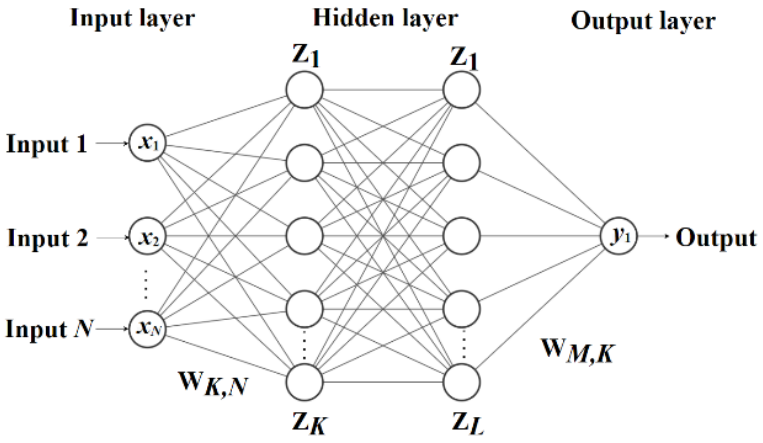

Fig. 2. The ANN model structure.

ANN is a biologically inspired computational model that constitutes a collection of hundred nodes of artificial neurons, each of which connected to others, that form a neural structure [26]. Figure 2 illustrates a diagram of a basic ANN model that the neurons are organized in layers of an input layer, multi hidden layers, and an output layer. At the first layer (the input layer), the neurons receive input signals of exogenous factors (called features), process them, and then transmit to the neurons in the consecutive layer (the hidden layer) connected to them. The transmitted signals are further transformed, and the final computations (called output) from the ANN model are delivered by the neurons of the output layer.

The computational capability of an ANN model is determined by the network structure, neuron's activation function, and learning rule. Equation 1 mathematically expresses the form of non-linear activation function that characterizes the artificial neurons:

$$z_i = f\left(w_x^{\mathrm{T}} x + b\right) \tag{1}$$

The variable z_i is the output from i^{th} hidden neuron, f is an activation function, $w_x \in R^{k\times 1}$ is the input weight factor, $x \in R^{k\times 1}$ is the input variable, and $b \in R$ is bias.

Equation 2 expresses the function of the neurons in the output layer:

$$y = f\left(w_y{}^{\mathrm{T}} z + b\right) \tag{2}$$

where y is the output variable, $w_y \in R^{k\times 1}$ is the output weight factor, and $b \in R$ is bias.

In order to apply the ANN method for problem solving, the ANN model does not require knowledge of the input data sources, but it can gather the knowledge by diagnosing the patterns and correlations in data and learning (or are trained) through experience. During training process, a number of weights of inter-connections among neurons and thresholds are to be adjusted until the error in the prediction is minimized and the network reaches the acceptable accuracy level.

3.2 Feature Selection

Solar radiation is stochastic and are influenced by climatic factors. Solar altitude (α_s) was commonly adopted as the input parameter by many physical and empirical radiation models [27]. Prior studies also indicated a large dependency of the radiation amount on sky prevalence [28]. In the solar research communities, several insolation indices were introduced for describing sky conditions. Since the global radiation was observed in most radiation stations, the clearness index (k_t), a ratio of the global radiation to its corresponding solar extraterrestrial, was broadly used to parameterize the sky condition from overcast through partly cloudy to clear skies. Diffuse fraction (k_d), defined as a ratio of the diffuse to global radiation, was another parameter adopted to differentiate cloudy sky from dark cloud to bright cloud. However, the diffuse radiation was less measured at solar radiation stations as compared to global radiation. Perez et al [29] recommended that the use of only one insolation parameter was not sufficient for the sky classification. Perez et al also introduced Perez's clearness index to improve the use of global radiation to describe sky condition.

Other than the use of radiation data, distribution patterns of luminance and radiance over the sky vault have also been used for the sky condition classification. In 2003, the Commission Internationale de l'Éclairage (CIE) proposed the fifteen standard sky luminance distributions to classify apparent sky condition. A ratio of zenith luminance to diffuse horizontal illuminance (L_z/E_{dv}) was introduced to parameterize the standard sky types [28]. Igawa *et al.* [30] also introduced an all-weather sky model that contained twenty patterns of the luminance distribution. The all-weather model employed an index namely normalized global solar radiation (N_{eg}) for the distribution classification. Performance of the CIE model and the Igawa model to classify Thai's sky were evaluated and the results showed the latter model could perform better. Also, it would imply that the nominalized global solar radiation well described the Thai's sky condition, as such this study included it as the model input. Below, Equations (3) and (4) express the mathematical formula of the solar altitude angle and normalized global solar radiation:

$$\alpha_s = \sin^{-1}\left[\cos\varphi\cdot\cos\delta\cdot\cos\omega + \sin\varphi\cdot\sin\delta\right] \tag{3}$$

where φ is latitude. δ is declination angle, and ω is hour angle.

$$N_{eg} = \frac{E_{eg,mea}}{E_{eg,ref}} \tag{4}$$

$$\begin{aligned} E_{eg,ref} = {} & -36.78\cdot\alpha_s^5 + 188.00\cdot\alpha_s^4 - 375.95\cdot\alpha_s^3 \\ & + 306.95\cdot\alpha_s^2 + 15.47\cdot\alpha_s + 0.83 \end{aligned} \tag{5}$$

In addition to the insolation indices mentioned above, numerous attempts of the ANN modeling included ambient temperature as input to forecast the solar radiation [27]. An advantage of inclusion ambient temperature (T_a) is due to its simplest available data source from meteorological stations. In this study, Table 3 shows the observed data and derived data considered for the input parameters of the ANN modeling.

Table 3. The available data at the meteorological station.

Data	Symbol	Unit
Observed data		
Global solar radiation	E_{eg}	W/m^2
Diffuse solar radiation	E_{ed}	W/m^2
Beam solar radiation	E_{eb}	W/m^2
Ambient air temperature	T_a	°C
Relative humidity	RH_a	%
Derived data		
Solar altitude angle	α_s	degree
Normalized global radiation	N_{eg}	-

The correlation coefficient is the statistic evaluator that can evaluate the relationship or association between two variables based on the covariance method [31]. To achieve an acceptable accuracy of the ANN solar modeling, selection of input parameters was performed by applying Pearson's correlation to identify the greatest influence among the various insolation and climate parameters. Equation (6) expresses mathematically

Pearson's correlation:

$$r_{xy} = \frac{\sum (x_i - \bar{x}) \cdot \sum (y_i - \bar{y})}{\sqrt{\sum (x_i - \bar{x})^2} \cdot \sqrt{\sum (y_i - \bar{y})^2}} \quad (6)$$

where r is Pearson correlation coefficient. x_i and y_i are the variable samples. $\bar{x}$ is the mean of values in x variables, and $\bar{y}$ is the mean of values in y variables.

Table 4 presents the evaluation results of the correlation among the input variables: N_{eg}, α_s, and T_a and the output variables: E_{eg}, and E_{ed}.

From the table, it could be observed a strong correlation between global radiation and solar altitude angle, providing correlation coefficient of 0.93. The correlation between the diffuse radiation and solar altitude angle was also as high as 0.82. When the correlations were evaluated between ambient temperature and the global and diffuse solar radiation, the values were also a strong correlation between 0.78 and 0.54. Moreover, normalized global radiation presented a moderate positive correlation between global solar radiation and diffuse solar radiation 0.73 and 0.57, respectively.

Based on the above evaluation results, the features input selected for the ANN models were solar altitude angle, normalized global solar radiation, and ambient temperature to forecast the one-hour ahead global radiation and diffuse radiation.

Table 4. Correlations analysis of the input-output variables of solar radiation forecasting modeling.

Parameter	E_{eg}	E_{ed}
N_{eg}	0.73	0.57
α_s	0.93	0.82
T_a	0.78	0.54

Table 5. Hyperparameters with tuning range.

Hyperparameter	Value/method
Epoch	500
Hidden layer No. 1	[8, 16, 32, 48, 64, 128]
Hidden layer No. 2	[8, 16, 32, 48, 64, 128]
Hidden layer No. 3	[8, 16, 32, 48, 64, 128]
Dropout	[0.0, 0.2, 0.4]
Learning rate	[0.001, 0.002]
Weight optimizer	Adam

3.3 Solar Modelling

The one-minute records from the station were averaged to the ten-minute data for the ANN modeling of the global and diffuse solar radiation forecasting. The data were then split into three sets of which the first sixty percent were used for the model training, the next ten percent for the model validation, and the last thirty percent for the model performance assessment.

Hyperparameter turning was carried out to optimize the model argument for maximizing the forecasting accuracy. The tuning approach could be categorized into manual tuning, grid search, and random search [32]. This work adopted the exhaustive grid search to try out all possible combinations of hyperparameter values to obtain the best set of values in the parameter search space. Table 5 gives the list of the hyperparameters with their tuning range.

In this study, Python with TensorFlow deep learning library version 2.4 was used as the programming tool to develop the forecasting model. Nonlinear problems required an algorithm or optimizer to determine the optimal solution by minimizing or maximizing the objective function. Among various optimizers, the stochastic gradient descent (SGD) was mostly used for black box models, but the solution converge was relatively slow as the SGD needed the forward and backward propagation for every subset of records. It was acknowledged that the Adaptive Gradient Algorithm (AdaGrad) worked well for sparse data, and the Root Mean Squared Propagation (RMSProp) for non-stationary data. The Adaptive moment estimation (Adam) combined advantages between AdaGrad and RMSProp, presenting one of the best stochastic optimizer techniques [33]. Therefore, this technique was adopted as the optimizer for weight optimization in the ANN modeling.

From the TensorFlow implementation, the forecasting model contained an input layer with α_s, N_{eg}, and T_a as the input variables. The number of neurons were 128, 64, and 32 in the first, second and third of the hidden layer, respectively. The activation function was the Rectified Linear Unit (ReLU). The loss function of mean square error (MSE) was used to train the ANN model. The learning rate was set at 0.001. In the training, the process would be terminated at 200 iterations or no significant change in the loss function.

For the model evaluation, K-fold cross-validation was employed to determine the model skill on unseen data. This technique divided the data into folds, training the model in each fold, and then average the performance

of each evaluation fold. In [34], it was shown that the K value of ten was the most common. Therefore, we also utilized the 10-fold cross-validation technique. As our data were time series, forward chaining idea was employed – meaning that the future data of each fold could not be trained to forecast past values. The first $(k-1)^{\text{th}}$ fold was used for training, while the k^{th} fold was used for evaluation. Therefore, in 10-fold cross-validation, we had only nine folds result to be averaged (see Fig. 3).

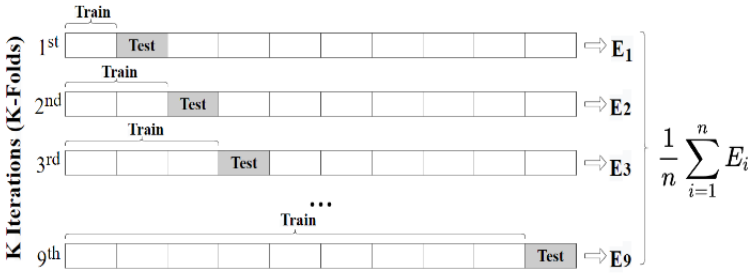

Fig. 3. Ten-folds cross validation with forward chaining.

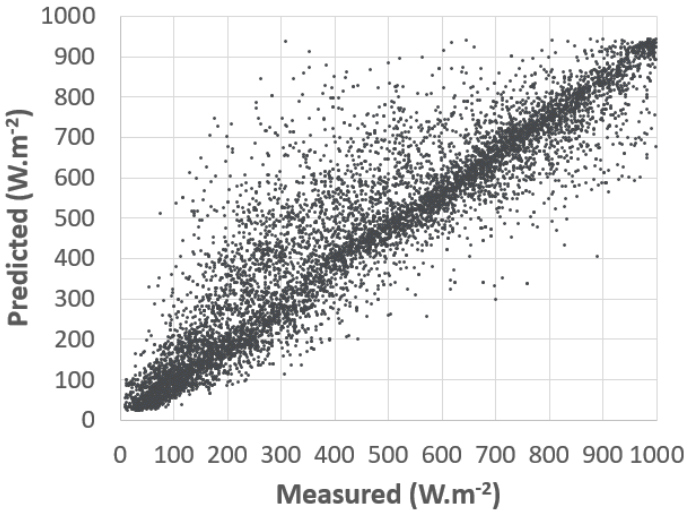

Fig. 4. Comparison of the measured global radiation with the forecasted values for the testing data.

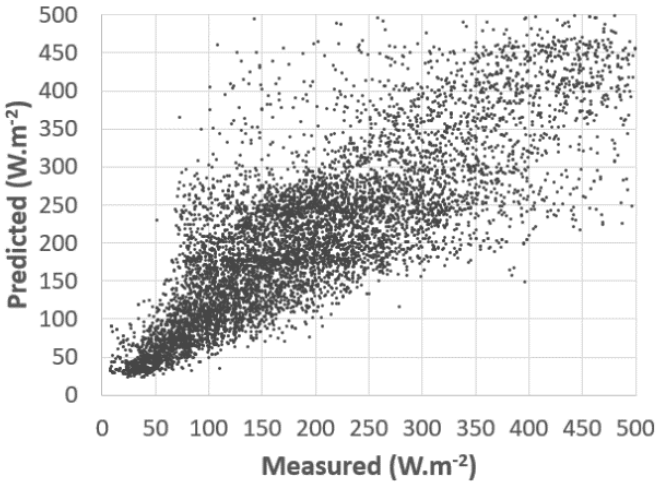

Fig. 5. Comparison of the measured diffuse radiation with the forecasted values for the testing data.

3.4 Performance Assessment

The developed ANN models were assessed their forecasting accuracy by using the test data set. The assessments were made by the standard parameters consisting of root mean squared error (*RMSE*), and mean bias error (*MBE*). The parameter definitions can be mathematically expressed by Equations (7)-(10):

$$RMSE = \sqrt{\frac{1}{n}\sum_{i=1}^{n}(p_i - a_i)^2}\,, \qquad (7)$$

$$nRMSE = \frac{RMSE}{\bar{a}_i}, \quad (8)$$

$$MBE = \frac{1}{n}\sum_{i=1}^{n}(p_i - a_i), \quad (9)$$

$$nMBE = \frac{MBE}{\bar{a}_i}, \quad (10)$$

where p_i and a_i are the forecasted and the actual solar radiation value, respectively.

The *RMSE* measures the spread of the forecasted values from the models around the actual values. The *MBE* indicates whether the models over-estimate (positive *MBE* value) or under-estimate (negative *MBE* value) the solar radiation for a long-term period. The *RMSE* and *MBE* are presented in the physical unit of W/m^2. The *nRMSE* and *nMBE* are the normalized values of the *RMSE* and *MBE* with respect to the average of the actual measured values.

- *Smart persistence model*

The persistence model presents the simplest way to forecast the solar radiation by which the future value is postulated to be equal to the previous one, as expressed by Equation (11):

$$\hat{x}_{t+h} = x_t. \quad (11)$$

The variable *x* in the equation stands for the global or the diffuse solar radiation. The subscripts *t* and *t+h* are denoted as the present time and the future time of the forecasting. Due to the simplicity of the model principle, it is obvious that the accuracy of the persistence model quickly drops with increasing future time horizon. In this regard, the smart persistence (SP) model was introduced as the improved version of which the forecasting takes into account the diurnal solar cycle by using the clear-sky solar radiation profile over the day [35]. The function form of the SP model can be expressed as:

$$\hat{x}_{t+h} = x_t \cdot \frac{x_{CS,t+h}}{x_{CS,t}}, \quad (12)$$

where $x_{CS,t+h}$ and $x_{CS,t}$ are the profile solar radiation under the clear sky condition at the future time *t+h* and the present time *t*, respectively.

In this study, the SP model was adopted as the reference for benchmarking the ANN model performance. However, it should be remarked that the clear-sky solar radiation profile was needed to establish for the model applicability. As mentioned in Section 3.2, the normalized global solar radiation (N_{eg}) was an indicator to parameterize the sky condition. According to the indicator's definition, the higher N_{eg} value would represent the clearer sky condition. Such that, in the step of the solar profile establishment, the measured global and diffuse solar radiation corresponding to the N_{eg} value greater than 0.9 were compiled from our database. The plot in Figure 6 shows the averaged values of the compiled radiation data with respect to the different five-degree ranges of the solar altitude from 0-90°. The two trend lines of the averaged values were plotted and given as the global and the diffuse solar radiation profiles of the clear sky.

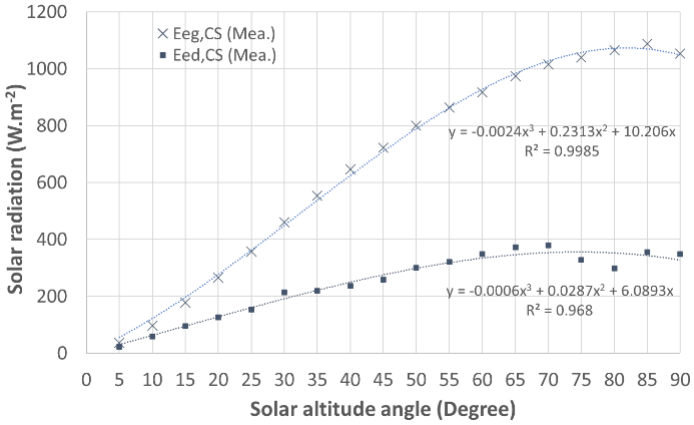

Fig. 6. The clear-sky global and diffuse radiation profiles.

Equations (13) and (14) express the empirical models of the clear-sky solar radiation profiles for the global ($E_{eg,CS}$) and the diffuse components ($E_{ed,CS}$), respectively:

$$E_{eg,CS} = -0.0024 \cdot \alpha_S^3 + 0.2313 \cdot \alpha_S^2 + 10.206 \cdot \alpha_S \ (R^2 = 0.998) \quad (13)$$

$$E_{ed,CS} = -0.0006 \cdot \alpha_S^3 + 0.0287 \cdot \alpha_S^2 + 6.0893 \cdot \alpha_S \ (R^2 = 0.968) \quad (14)$$

The coefficient of determination (R^2) of the regression was given as shown. With the equations, when the forecasting time was known, the corresponding solar altitude and the clear-sky solar radiation profile could be determined, accordingly.

- *Global radiation*

Although the seasonal variation over year was not obvious in the tropical climate of the study site, the model performance was assessed for the two distinct periods that were the wet period during eight months from March to

October, and the dry period of four months from November to February.

The upper section of Table 6 summarizes the statistics of the solar radiation for the two periods. As shown, the global radiation in the wet period had an average value of 498.67 W/m^2 with the standard deviation of 301.95 W/m^2. The global radiation in the dry period was marginally lower in terms of both its amount and variation as compared to the wet period.

The SP model forecasted the one-hour ahead global radiation in the wet period with the *RMSE* value of 169.49 W/m^2, supposing the *nRMSE* value of 40.36%. The *nMBE* value was obtained at -18.75% (*MBE*=-78.74W/m^2), indicating that the forecasted values from the SP model tended to underestimate the actual values. Considering the values of the *nRMSE* (39.32%) and the *nMBE* (-23.08%) for the dry period, the forecasting performance of the SP model was quite comparable to that of the wet period. Realizing the distinct sky condition between the wet period and the dry period as described in Section 2.3, the comparable *nRMSE* values of the two assessment periods implied that the solar global radiation profile of the clear sky was also applicable for other sky conditions.

Table 6 shows that the ANN model had the *nRMSE* value of 26.90% and the *nMBE* value of 2.47% for the wet period and had the *nRMSE* value of 23.90% and the *nMBE* value of 0.11% for the dry period. When benchmarked with the SP model, the ANN model possessed the smaller *nRMSE* and *nMBE* values for all cases, deducing the superior forecasting performance of the ANN model. The significant improvement of the ANN model performance was due to the inclusion of the derived N_{eg} indicator as the model input for sky parameterization. The forecasting performance of the ANN model was also observed to improve in case of the dry period.

Table 6. Performance evaluation of the developed ANN forecasting models.

Parameter (W.m^{-2})	Global radiation			Diffuse radiation		
	Wet period	Dry period	Whole year	Wet period	Dry period	Whole year
Measurement						
Mean	498.67	443.73	481.08	234.07	189.42	219.78
Standard deviation	301.95	258.88	289.99	138.64	105.97	130.75
Smart Persistence (SP) Model						
Prediction						
Mean	419.93	360.50	400.91	184.18	148.43	172.74
Standard deviation	304.18	262.61	292.83	147.96	111.10	138.25
Performance						
MBE (W/m^2)	-78.74	-83.20	-80.16	-49.90	-40.99	-47.05
nMBE (%)	-18.75	-23.08	-20.00	-27.09	-27.62	-27.24
RMSE (W/m^2)	169.49	141.76	161.14	112.66	81.89	103.81
nRMSE (%)	40.36	39.32	40.19	61.17	55.17	60.1
Artificial Neural Network (ANN) Model						
Prediction						
Mean	511.31	444.22	489.83	254.23	204.50	238.31
Standard deviation	266.83	231.22	257.88	129.84	100.79	123.50
Performance						
MBE (W/m^2)	12.65	0.49	8.75	20.16	15.08	18.53
nMBE (%)	2.47	0.11	1.79	7.93	7.37	7.78
RMSE (W/m^2)	137.54	106.15	128.33	91.94	72.83	86.28
nRMSE (%)	26.90	23.90	26.20	36.16	35.61	36.21

The aggregated results of the whole year assessment were also provided in Table 6. The *RMSE* and *MBE* of the ANN models were 128.33 W/m^2 and 8.75 W/m^2, corresponding to the *nRMSE* and *nMBE* values of 26.20% and 1.79%, respectively.

In this study, the performance of the developed ANN models was also compared to some models selected from the literature. Benali *et al.* [35] developed the artificial neural network (ANN) model, and the random forest (RF) model to forecast the one-hour ahead global and diffuse solar radiation in France. The smart persistence (SP) model was used for the benchmarking. The study results of the model performance in terms of *nRMSE* were reproduced in Table 7.

Voyant and Notton [36] used the global radiation data from Ajacco, Spain to develop the forecasting models using three techniques *i.e.* the autoregression (AR) model, the ANN model, and the stochastic persistence (StP) model. However, the scope of this work limited to only the global radiation modeling. For Alonso-Montesinos's work [37], the forecasting model was developed based on the cloud motion vector (CMV) where the satellite images were employed for the model input to determine the cloud position in a considered time horizon. All the model

performance in Table 7 were evaluated on the annual basis.

In summary, the results in Table 7 show that the author's ANN model performance of the global radiation forecasting did well compared to those models of Benali [35], Voyant [36], where the *nRMSE* values were within a range of 19.65-26.90%. No explicit difference of the prediction performance could be observed among the SP, ANN, RF, and StP models. However, the Alonso-Montesinos' study presented a significant performance improvement of the forecasting model with the input of the cloud motion data.

Table 7. Forecasting performance of the proposed models by other authors.

Authors	Model	Normalized root means square error (*nRMSE*)	
		Global radiation	Diffuse radiation
Benali *et al.* [35]	SP	21.67	63.64
	ANN	22.57	40.99
	RF	19.65	35.08
Voyant and Notton [36]	AR	19.54	na.
	ANN	19.29	na.
	StP	19.88	na.
Alonso-Montesinos and Batlles [37]	CMV	10.27	16.40

- *Diffuse radiation*

In Table 6, the diffuse horizontal radiation in the wet period was at an average of 234.07 W/m^2, corresponding to 46.94% of the average global radiation. The standard deviation was calculated at 138.64 W/m^2, indicating the large variation of the diffuse component.

The *MBE* in Table 6 exhibits that the SP model largely underestimated the diffuse radiation by 49.9 W/m^2 for the wet period and 40.99 W/m^2 for the dry period, corresponding to the *nMBE* value of around -27.0%. The evaluation also shows that the *nRMSE* value was 61.17% for the wet period and slightly improved to 55.17% for the dry period. The results seemed to be distinct from the previous case that the diffuse radiation profile of the clear sky was not applicable for partly cloudy and cloudy sky, hence resulting in the forecasting the worst in the wet period. Overall, the SP model performed worsen forecasting of the diffuse than the global radiation.

For the developed ANN model, the forecasted diffuse radiation values were slightly higher than the actual values by 20.16 W/m^2 in the wet period and by 15.08 W/m^2 in the dry period (*nMBE* of about 7.4%). The ANN model had the *nRMSE* value of 36.16% for the wet period and 35.61% for the dry period, indicating the forecasting accuracy did well compare for both periods. Benchmarking with the SP model, the ANN model possessed the better accuracy of forecasting the diffuse radiation.

Comparing the forecasting performance of the diffuse radiation among the different models, the results in Table 7 indicate the author's ANN model well compared to the models from Benali *et al.* study, but it did worse than the Alonso-Montesinos' model.

3.5 Application of the Forecasted Horizontal Data to Predict the Total Solar Radiation on Vertical Surface

Incident solar radiation on building facades ($E_{t\beta}$) is the primary data for determining the building envelope heat gain. The incident radiation consists of the two basic components: the direct ($E_{b\beta}$) and the diffuse ($E_{d\beta}$) radiation. The amount of $E_{b\beta}$ can be determined by multiplying the beam normal radiation (E_{eb}) with its incidence angle on the surface. However, the calculation is more complicated for $E_{d\beta}$, as the sky luminance distribution is anisotropic, and the facades are positioned to face only part of the sky hemisphere. In our prior study, a localized Perez's model was proposed to determine the diffuse radiation from the sky on vertical surfaces for Bangkok. In the procedure, the two horizontal data of the global and the diffuse solar radiation are required as the input. The detailed description of the model was given in [7].

In order to demonstrate a benefit of the developed ANN models, the paired values of the forecasted horizontal data from the models were used to further predict the total radiation on the vertical facades with the assistance of the Perez's transposition model. The calculated results were compared to the real measurement from the station and benchmarked with that obtained from the same calculation procedure but using the forecasted data from the SP model.

The solar radiation on the south orientation was chosen as the study case. Figure 7 shows the plots of the measured radiation at the station for seven consecutive days during 4-10 December 2021. The plots were also superimposed by the forecasted values from the ANN models and the SP models.

As the observation was made in the dry period that the sky was clear for most daytime and the sun traveled due south with low elevation angle, the total radiation on the south reached 800 W/m^2, as illustrated in Figure 7(a). However, the stochastic variation of the diffuse radiation in Figure 7(b) indicated the presence of moving clouds which was more pronounced on the day 2, 3, 6, and 7 of the observation. The total radiation of the south orientation is given in Figure 7(c) and the influence of the clouds was obvious.

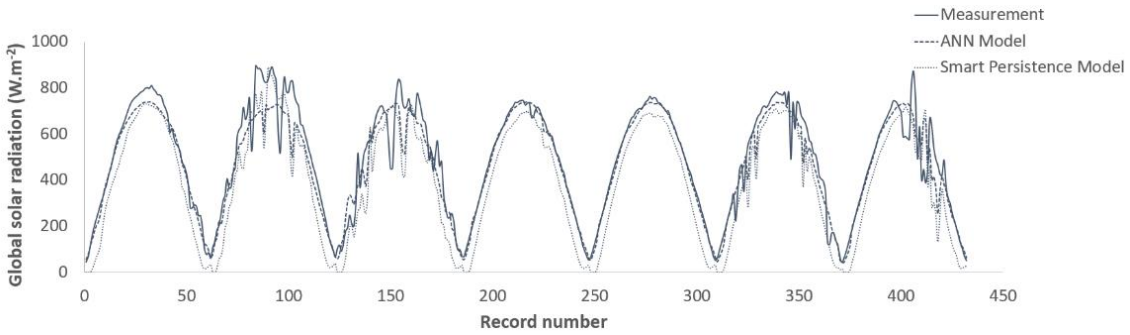

(a) Forecasted global radiation.

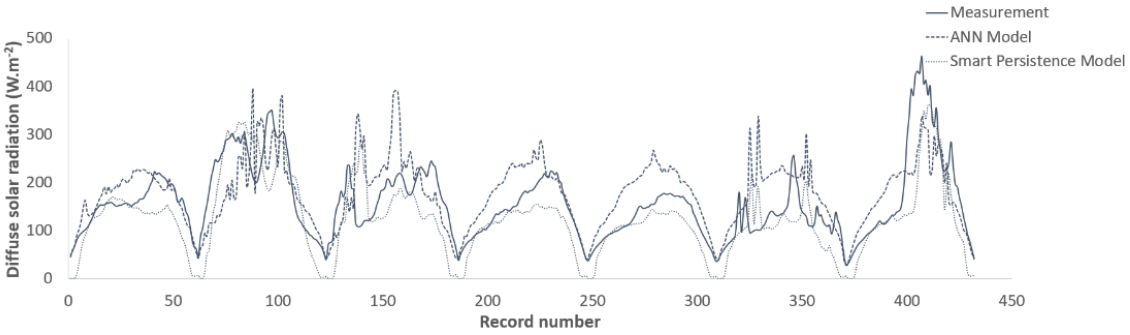

(b) Forecasted diffuse horizontal radiation.

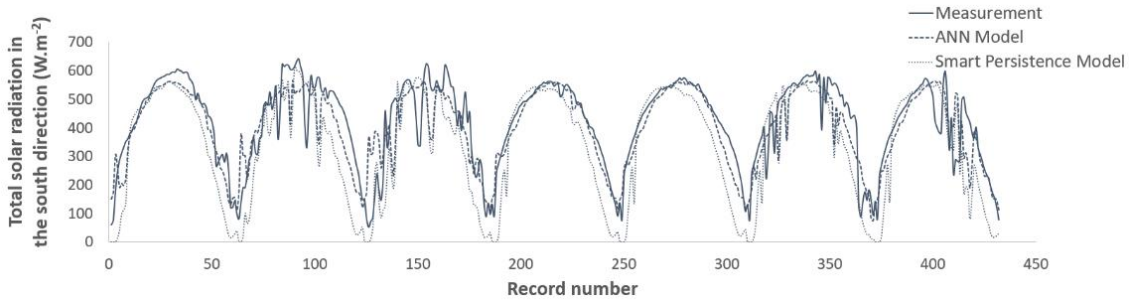

(c) Forecasted total radiation on south orientation.

Fig. 7. Forecasting of the total solar radiation on south orientation during 4-10 December 2021.

Table 8 summarizes the experimental results of forecasting the total radiation on the south using the horizontal data from the ANN models. For the seven-day observation, the mean value of the total radiation was 424.00W/m^2. The standard deviation was 151.98W/m^2. The forecast using the data from the SP model presented a large error with the *nMBE* of -24.96% and *nRMSE* of 37.97%. The results in the table show that the ANN model could give the lower values of both *nMBE* and *nRMSE*, indicating the better forecasting accuracy of the ANN model.

For the analysis using the whole data, the mean value of the total radiation on the south reduced to 190.74W/m^2, as the data included all sky conditions (not only clear sky) and the period that the sun traveled due north so only the diffuse radiation presented on the south façade. It was again that the ANN model could perform better than the SP model. This was resulted from that the ANN model forecasted the diffuse horizontal radiation more accurately than the SP model.

4. CONCLUSION

The tropical global and diffuse solar radiation of Bangkok was high and largely variable. The monthly average hourly mean value of the global radiation was higher than 700 W/m^2 during noon throughout the wet period from March to October. The diffuse radiation was above 350 W/m^2 in the raining season (August-October). Due to the presence of clouds for most time over years, the diffuse radiation shared up to almost 50% of the global solar radiation. As observed in the iso-contour plots in the appendix, although the seasonal changes were not clearly distinct in the study location, its influence on the solar radiation variation could be noticed.

The artificial neural network (ANN) models were developed for the global and diffuse solar radiation forecasting for one-hour ahead. Based on the correlation testing, the three parameters of the solar altitude angle, the normalized global radiation index and the ambient air temperature were chosen as the model's input.

The proposed ANN model performance was assessed by using the two common statistic parameters. The results

showed that the ANN models could forecast the global radiation with the *nMBE* of 1.79% (*MBE*=8.75 W/m^2) and *nRMSE* of 26.20% (*RMSE*=128.33 W/m^2). For the diffuse radiation forecasting, the *nMBE* and *nRMSE* were assessed at 7.78% and 36.21%, respectively. The models forecasted the global radiation more accurately than the diffuse radiation. Our developed model performance was also compared with the selected models of other authors. Although the solar radiation in the tropics were largely variant over year, the forecasting performance was found to be well compared.

Table 8. Experimental results of forecasting the total solar radiation on the south using the ANN models.

Parameter (W.m^{-2})	Total solar radiation	
	7-day observation	Whole data
Measurement		
Mean	424.00	190.74
Standard deviation	151.98	147.80
Smart Persistence (SP) Model		
Prediction		
Mean	339.32	151.69
Standard deviation	195.55	138.33
Performance		
MBE (W/m^2)	-84.69	-39.05
nMBE (%)	-24.96	-25.75
RMSE (W/m^2)	128.84	80.67
nRMSE (%)	37.97	53.18
Artificial Neural Network (ANN) Model		
Prediction		
Mean	403.99	207.62
Standard deviation	134.89	141.68
Performance		
MBE (W/m^2)	-20.02	16.88
nMBE (%)	-4.96	8.13
RMSE (W/m^2)	73.68	70.81
nRMSE (%)	18.24	34.11

This study demonstrated the deployment of the developed ANN models together with the localized Perez's transposition model to predict the solar radiation on the vertical surfaces. The evaluation showed that the prediction for the south-facing plane could be achieved with the *nMBE* of 8.13% and *nRMSE* of 34.11%. The developed ANN models performed better prediction than the smart persistence model for all cases.

For future work, the potential improvement of the model performance could be suggested by expanding the range of the hyperparameter turning. The hybrid of different artificial intelligence techniques can offer the enhancement of the forecasting accuracy.

NOMENCLATURE

E_{eg}	global solar radiation
E_{ed}	diffuse horizontal radiation
E_{eb}	beam normal radiation
T_a	air dry-bulb temperature
RH_a	air relative humidity
V_a	wind velocity
z_i	output from hidden neuron
w_x	input weight
b	bias
y	output
w_y	output weight
α_s	solar altitude angle
k_t	clearness index
k_d	diffuse fraction
L_z	zenith luminance
E_{dv}	diffuse horizontal illuminance
N_{eg}	normalized global solar radiation
φ	latitude
δ	declination angle
ω	hour angle
$E_{eg,mea}$	measurement global solar radiation
$E_{eg,ref}$	reference global solar radiation
$x_{cs,t}$	profile radiation under the clear sky condition at the present time t
$x_{cs,t+h}$	profile radiation under the clear sky condition at the future time $t+h$
$E_{eg,CS}$	clear-sky global radiation profile
$E_{ed,CS}$	clear-sky diffuse radiation profile
$E_{t\beta}$	incident solar radiation on tilted plane

$E_{b\beta}$ direct radiation on tilted plane

$E_{d\beta}$ diffuse radiation on tilted plane

ACKNOWLEDGEMENT

This research project was supported by National Science, Research and Innovation Fund, FF 2565: FRB 650048/0164. The authors also express their gratitude to The Joint Graduate School of Energy and Environment (JGSEE), King Mongkut's University of Technology Thonburi and the Center of Excellence on Energy Technology and Environment (CEE), Ministry of Higher Education, Science (MHESI), Research and Innovation.

REFERENCES

[1] Abergel T., Dean B., and Dulac J., 2017. *Towards a zero-emission, efficient, and resilient buildings and construction sector*. .

[2] Das U.K., Tey K.S., Seyedmahmoudian M., Mekhilef S., Idris M.Y.I., Deventer W.V., Horan B., Stojcevskid A. 2018. Forecasting of photovoltaic power generation and model optimization: A review. *Renewable and Sustainable Energy Reviews* 81(1): 912–928.

[3] Urraca R., Sanz-Garcia A., and Sanz-Garcia I., 2020. BQC: A free web service to quality control solar irradiance measurements across Europe. *Solar Energy* 211: 1–10.

[4] Mohammad S.T., Al-Kayiem H.H., Aurybi M.A., and Khlief A.K., 2020. Measurement of global and direct normal solar energy radiation in Seri Iskandar and comparison with other cities of Malaysia. *Case Studies in Thermal Engineering* 18: 100591.

[5] Wu J. and C.K. Chan. 2013. Prediction of hourly solar radiation with multi-model framework. *Energy Conversion and Management* 76: 347–355.

[6] Rumbayan M., Abudureyimu A., and Nagasaka K., 2012. Mapping of solar energy potential in Indonesia using artificial neural network and geographical information system. *Renewable and Sustainable Energy Reviews* 16(3): 1437–1449.

[7] Chirarattananon S., Chaiwiwatworakul P., and Pattanasethanon S., 2002. Daylight availability and models for global and diffuse horizontal illuminance and irradiance for Bangkok. *Renewable Energy* 26(1): 69–89.

[8] Wang H., Lei Z., Zhang X., Zhou B., and Peng J., 2019. A review of deep learning for renewable energy forecasting. *Energy Conversion and Management* 198: 111799.

[9] Mathiesen P. and J. Kleissl. 2011. Evaluation of numerical weather prediction for intra-day solar forecasting in the continental United States. *Solar Energy* 85(5): 967–977.

[10] Gamarro H., Gonzalez J.E., and Ortiz L.E., 2019. On the assessment of a numerical weather prediction model for solar photovoltaic power forecasts in cities. *Journal of Energy Resources Technology, Transactions of the ASME* 141 (6): 061203.

[11] Böök H. and A.V. Lindfors. 2020. Site-specific adjustment of a NWP-based photovoltaic production forecast. *Solar Energy* 211: 779–788.

[12] Tolstykh M.A. and A.V. Frolov. 2005. Some current problems in numerical weather prediction. *Izvestiya - Atmospheric and Ocean Physics* 41(3): 285–295.

[13] Diagne M., David M., Lauret P., Boland J., and Schmutz N., 2013. Review of solar irradiance forecasting methods and a proposition for small-scale insular grids. *Renewable and Sustainable Energy Reviews* 27: 65–76.

[14] Ibrahim S., Daut I., Irwan Y.M., Irwanto M., Gomesh N., and Farhana Z., 2012. Linear regression model in estimating solar radiation in perlis. *Energy Procedia* 18: 1402–1412.

[15] Mbaye A., Ndiaye M., Ndione D.M., Diaw M., Traore V., Ndiaye A., Sylla M.C., Aidara M.C., Diaw V., Traore A., and Ndiaye P., 2019. ARMA model for short-term forecasting of solar potential : application to a horizontal surface on Dakar site. *Materials and Devices* 4(1): 1103.

[16] Pazikadin A.R., Rifai D., Ali K., Malik M.Z., Abdalla A.N., and Faraj M.A., 2020. Solar irradiance measurement instrumentation and power solar generation forecasting based on Artificial Neural Networks (ANN): A review of five years research trend. *Science of the Total Environment* 715: 136848.

[17] Ağbulut Ü., Gürel A.E., and Biçen Y., 2021. Prediction of daily global solar radiation using different machine learning algorithms: Evaluation and comparison. *Renewable and Sustainable Energy Reviews* 135: 110114.

[18] Ghimire S., Deo R.C., Downs N.J., and Raj N., 2019. Global solar radiation prediction by ANN integrated with European Centre for medium range weather forecast fields in solar rich cities of Queensland Australia. *Journal of Cleaner Production* 216: 288–310.

[19] Notton G., Batlles C., Fouilloy A., Duchaud J.L., and Nivet M.L., 2019. Some applications of ANN to solar radiation estimation and forecasting for energy applications. *Applied Sciences (Switzerland)* 9 (1): 209.

[20] Notton G., Paoli C., Ivanova L., Vasileva S., and Nivet M.L., 2013. Neural network approach to estimate 10-min solar global irradiation values on tilted planes. *Renewable Energy* 50: 576–584.

[21] Premalatha N. and A. Valan Arasu. 2016. Prediction of solar radiation for solar systems by using ANN models with different back propagation algorithms. *Journal of Applied Research and Technology* 14(3): 206–214.

[22] Alam S., Kaushik S.C., and Garg S.N., 2009. Assessment of diffuse solar energy under general sky condition using artificial neural network. *Applied Energy* 86(4): 554–564.

[23] Waewsaka J., Chancham C., Mani M., and Gagnon, Y., 2014. Estimation of monthly mean daily global solar radiation over Bangkok, Thailand using artificial neural networks. *Energy Procedia* 57: 1160–1168.

[24] Paoli C., Voyant C., Muselli M., and Nivet M.L., 2010. Forecasting of preprocessed daily solar radiation time series using neural networks. *Solar Energy* 84(12): 2146–2160.

[25] Xue X., 2017. Prediction of daily diffuse solar radiation using artificial neural networks. *International Journal of Hydrogen Energy* 42(47): 28214–28221.

[26] Kumar E.P. and E.P. Sharma. 2014. Artificial Neural Networks-A Study. *International Journal of Emerging Engineering Research and Technology* 2 (2): 143–148.

[27] Sobri S., Koohi-Kamali S., and Rahim N.A., 2018. Solar photovoltaic generation forecasting methods: A review. *Energy Conversion and Management* 156: 459–497.

[28] Chaiwiwatworakul P. and S. Chirarattananon. 2013. Luminous efficacies of global and diffuse horizontal irradiances in a tropical region. *Renewable Energy* 53: 148–158.

[29] Perez R., Seals R., Ineichen P., Stewart R., and Menicucci D., 1987. A new simplified version of the perez diffuse irradiance model for tilted surfaces. *Solar Energy* 39(3): 221–231.

[30] Igawa N., 2014. Improving the All Sky Model for the luminance and radiance distributions of the sky. *Solar Energy* 105: 354–372.

[31] Jebli I., Belouadha F.Z., Kabbaj M.I., and Tilioua A., 2021. Prediction of solar energy guided by pearson correlation using machine learning. *Energy* 224: 120109.

[32] Yu T. and H. Zhu. 2020. Hyper-Parameter Optimization: A Review of Algorithms and Applications. 1–56.

[33] Kingma D.P. and J.L. Ba. 2015. Adam: A method for stochastic optimization. In *3rd Int. Conf. Learn. Represent. ICLR 2015 - Conf. Track Proc.* pp. 1–15.

[34] Chen C., Duan S., Cai T., and Liu B., 2011. Online 24-h solar power forecasting based on weather type classification using artificial neural network. *Solar Energy* 85(11): 2856–2870.

[35] Benali L., Notton G., Fouilloy A., Voyant C., and Dizene R., 2019. Solar radiation forecasting using artificial neural network and random forest methods: Application to normal beam, horizontal diffuse and global components. *Renewable Energy* 132: 871–884.

[36] Voyant C. and G. Notton. 2018. Solar irradiation nowcasting by stochastic persistence: A new parsimonious, simple and efficient forecasting tool. *Renewable and Sustainable Energy Reviews* 92: 343–352.

[37] Alonso-Montesinos J. and F.J. Batlles. 2015. Solar radiation forecasting in the short- and medium-term under all sky conditions. *Energy* 83: 387–393.

APPENDIX

Table A.1. Monthly standard deviations of the measured global radiation (W/m^2).

Time	M1	M2	M3	M4	M5	M6	M7	M8	M9	M10	M11	M12
1	-	-	-	-	-	-	-	-	-	-	-	-
2	-	-	-	-	-	-	-	-	-	-	-	-
3	-	-	-	-	-	-	-	-	-	-	-	-
4	-	-	-	-	-	-	-	-	-	-	-	-
5	-	-	-	-	-	-	-	-	-	-	-	-
6	-	2	10	25	39	37	28	21	23	21	15	6
7	43	47	68	79	94	93	90	70	88	87	74	52
8	92	79	106	126	155	133	147	123	146	144	123	117
9	125	114	149	187	217	161	185	162	205	195	158	152
10	135	107	170	216	234	199	216	212	239	236	190	167
11	171	91	169	226	236	210	223	230	254	260	212	190
12	187	101	146	243	255	241	236	229	256	278	217	193
13	179	107	137	235	220	230	241	225	245	284	217	186
14	163	115	125	232	212	210	231	218	216	254	182	154
15	137	109	118	181	163	198	200	193	175	185	137	125
16	98	84	106	136	123	153	150	144	122	101	82	81
17	57	63	75	86	87	85	85	78	66	44	37	38
18	7	16	22	24	32	33	31	23	11	2	0	1
19	-	-	-	-	-	-	-	-	-	-	-	-
20	-	-	-	-	-	-	-	-	-	-	-	-
21	-	-	-	-	-	-	-	-	-	-	-	-
22	-	-	-	-	-	-	-	-	-	-	-	-
23	-	-	-	-	-	-	-	-	-	-	-	-
24	-	-	-	-	-	-	-	-	-	-	-	-

Table A.2 Monthly standard deviations of the measured diffuse horizontal radiation (W/m^2).

Time	M1	M2	M3	M4	M5	M6	M7	M8	M9	M10	M11	M12
1	-	-	-	-	-	-	-	-	-	-	-	-
2	-	-	-	-	-	-	-	-	-	-	-	-
3	-	-	-	-	-	-	-	-	-	-	-	-
4	-	-	-	-	-	-	-	-	-	-	-	-
5	-	-	-	-	-	-	-	-	-	-	-	-
6	-	2	7	19	28	28	29	42	18	17	12	5
7	29	32	35	41	50	52	46	49	49	45	38	32
8	46	41	56	67	75	85	76	82	82	75	62	59
9	121	61	84	101	101	147	110	129	133	104	93	124
10	197	88	93	112	117	153	140	148	143	129	113	167
11	126	84	95	130	131	174	153	141	152	127	118	133
12	118	89	97	137	147	167	160	141	151	121	110	120
13	131	85	97	131	124	155	150	139	142	125	101	122
14	184	79	81	116	124	150	134	144	127	109	82	137
15	160	67	65	105	97	125	111	135	104	89	70	107
16	73	44	48	71	66	83	78	99	72	62	43	58
17	35	27	32	44	44	46	51	58	45	35	30	30
18	6	21	17	18	23	26	28	51	10	2	0	1
19	-	-	-	-	-	-	-	-	-	-	-	-
20	-	-	-	-	-	-	-	-	-	-	-	-
21	-	-	-	-	-	-	-	-	-	-	-	-
22	-	-	-	-	-	-	-	-	-	-	-	-
23	-	-	-	-	-	-	-	-	-	-	-	-
24	-	-	-	-	-	-	-	-	-	-	-	-

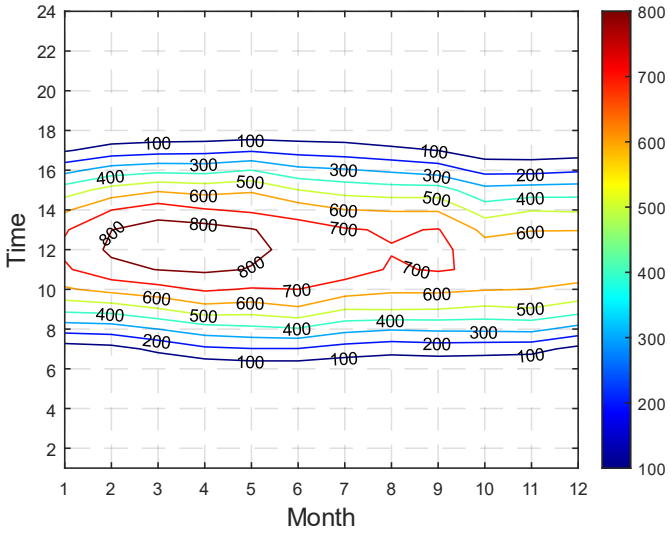

Fig. A.1. Contour plot of the global radiation.

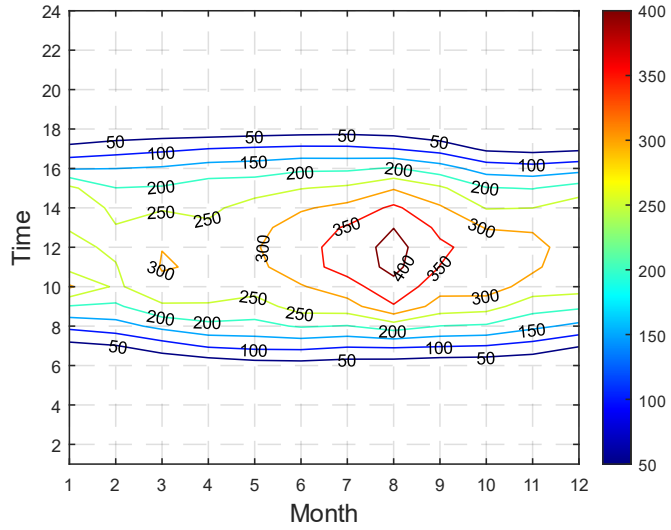

Fig. A.2 Contour plot of the diffuse radiation.

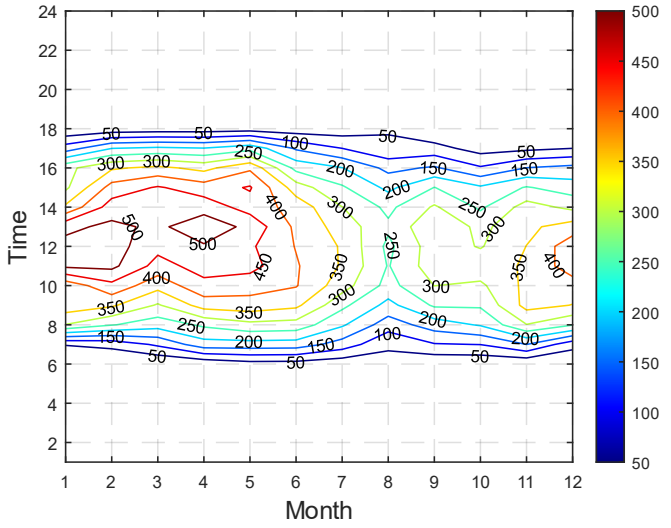

Fig. A.3 Contour plot of the beam radiation.